Strong Influence of Off-site Symmetry Positions of Hydrogen Atoms in ScH_3 hcp Phases

T. Pakornchote,[1,2] T. Bovornratanaraks,[1,2,a)] S. Vannarat,[3] and U. Pinsook[1,2,b)]

[1)] *Department of Physics, Faculty of Science, Chulalongkorn University, Bangkok, Thailand*

[2)] *ThEP, Commission on Higher Education, 328 Si-Ayutthaya Road, 10400 Bangkok, Thailand*

[3)] *Large-Scale Simulation Research Laboratory, Thailand National Electronics and Computer Technology Center, Pathumthani, Thailand*

(Dated: 16 June 2015)

We investigate the wave-like arrangements of H atoms around metal plane (H_m) in the ScH_3 hcp phase by using the *ab-initio* method. We found that only $P6_3/mmc$, $P\bar{3}c1$, $P6_3cm$ and $P6_3$ phases are energetically favorable. The wave-like arrangement allows the off-site symmetry positions of the H atoms, and leads to substantial changes in the pair distribution between Sc and H atoms which are associating with the changes in the electronic structure in such a way that the total energy is lowering. The symmetry breaking from $P6_3mmc$ is also responsible for the band gap opening. In the $P6_3$ structure, the calculated band gap is 0.823 eV and 1.223 eV using GGA and sX-LDA functionals, respectively. This band gap can be compared with 1.7 eV derived from the optical measurement and 1.55 eV from the HSE06 calculation. Thus, the broken symmetry structures can be viewed as Peierls distortion of the $P6_3/mmc$ structure. Furthermore, we found that only the $P6_3$ structure is dynamically stable, unlike YH_3 where the $P6_3cm$ structure is also stable. The stability of $P6_3$ comes from sufficiently strong interactions between two neighboring H atoms at their off-site symmetry positions, i.e. near the metal plane and near the tetragonal site. The $P6_3$ phonon density of states is in good agreement with the data from the neutron experiment.

[a)]Electronic mail: thiti.b@chula.ac.th

[b)]Electronic mail: udomsilp.p@chula.ac.th

I. INTRODUCTION

Rare-earth metal hydride (REH_x) compounds have been found to be a switchable metal-insulator material under variation of the H content. The electronic property changes from a metal in dihydrides to an insulator in trihydrides, and the corresponding structure changes from the fcc to the hcp phase.[1–3] Under high pressure, the stoichiometry ratio of REH_x increases up to x = 3, and the crystal structure transform as the following typical sequences; hcp $\rightarrow$ intermediate $\rightarrow$ fcc $\rightarrow$ hcp $\rightarrow$ $Cmcm$[4–12]. The second appearance of the hcp phase at higher pressure is different from the first appearance at lower pressure by the arrangement of H atoms.

There were several investigations on the arrangements of the H atoms in the YH_3 hcp phase (the first appearance at lower pressure), and their influence on the electronic and dynamical properties[13–21]. The structure of the YH_3 hcp phase was suggested to be similar to the HoD_3 structure[22], which has six yttrium atoms in the unit cell, thus its Brillouin zone is one-third of the $P6_3/mmc$ hcp unit cell with 30° (anti)clockwise rotation about the c axis. The K point folds up three times into the Γ point. Its H atoms can be categorized into two groups, i.e. the H atom near a tetrahedral site (H_t) and the H atom around a metal plane (H_m). The on-site symmetry position of the tetrahedral site is located at the center of a tetrahedron with one Sc atom at each corner. Thus H_t is surrounded by four Sc atoms. On the other hand, the H_m atom is surrounded by three Sc atoms. There are three possible positions for each H_m atom, i.e. above, under or on the metal plane. The position on the metal plane is the on-site symmetry position, whereas the other two positions are the off-site symmetry positions. According to these different H atoms arrangements, the symmetry can varies from 24 operations in the $P6_3/mmc$ phase (where all the H_m atoms are at their on-site symmetry positions) to, for example, 12 operations in the $P\bar{3}c1$ phase. Gelderen et al proposed that the $P6_3cm$ and $P6_3$ phases are more energetically favorable and dynamically stable than the $P\bar{3}c1$ phase which has the phonon softening modes around the Γ point[20]. Furthermore, the phonon DOS from the neutron powder diffraction (NPD) experiment[21] was in good agreement with the average phonon DOS of $P6_3$ and $P6_3cm$. They also suggested that $P\bar{3}c1$ could be the mean structure of the YH_3 hcp phase.

For ScH_3, the NPD experiment showed that the Sc atoms also form a hcp structure[23]. The $P6_3/mmc$ structure was used to fit the NPD data but the experimental evidence pointed

out that the arrangement of the H atoms is more complicated. Antonov et al found that the H_m atoms must distribute around the metal planes, i.e. occupy some off-site symmetry positions. They also suggested that the structure of the ScH_3 hcp phase would be similar to that of YH_3. Moreover, the ScH_3 hcp phase found to be a semiconductor, the same as YH_3, with the band gap of approximately 1.7 eV at ambient pressure by extrapolating from the optical experiment data[24].

In this work, we examined all possible arrangements of the H_m atoms in the ScH_3 hcp phase in a sufficiently large supercell with six Sc atoms, and their influence on the energy and dynamical properties. Our finding confirms that the broken symmetry structures cause the band gap opening, and result in the energy reduction. This can be viewed as Peierls distortion of $P6_3/mmc$. Furthermore, we investigated the dynamical stability of the hcp phase. We found that the strong interaction between off-site symmetry positions of H_t and H_m play a crucial role in the stability of the hcp phase.

This paper is organized as follows; the calculation method is explained in section II. The symmetry breaking structures are described in section III as well as their energetical comparison. The relation between the structural and electronic properties is discussed in section IV. Their dynamical stability are discussed and compared with the recent experimental data[23] in section V.

II. METHOD

We use CASTEP code based on the density functional theory (DFT) using the plane-wave method to study the properties of the ScH_3 hcp phases[25–28]. The Perdew-Burke-Ernzerhof (PBE) exchange-correlation functional[29] is chosen to calculate the energy and the physical properties such as geometry and phonons. The ultrasoft pseudopotential based on Vanderbilt theory[30] is chosen for the Sc atom with $3d^1\ 3s^2\ 3p^6\ 2s^2$ electronic configuration. A sufficiently large supercell with six Sc atoms is chosen in order to accommodate most of the hcp phases found in YH_3. A larger supercell is beyond our scope. The lattice parameters and the atomic positions are relaxed to their optimum structure using the Broyden-Fletcher-Goldfarb-Shanno (BFGS) method[31]. For the accuracy of the calculation, the convergence test is performed, so that the variation of energy is less than 1.6 meV. The optimum parameters are as follows; the energy cutoff (E_c) is 600 eV, and the spacing between k-mesh grid

using Monkhorst-Pack scheme[32,33] is ≈ 0.02 Å^{-1}. The supercell of 192 atoms (48 Sc atoms) is used for the phonon calculation with the finite displacement method[34].

We scope ourselves to the GGA regime. However, the bandgap accuracy can be improved by explicitly including the screened exchange (sX) interaction[35]. The sX gives partial correction to the electron self-energy, and hence improve the excited states. We apply sX-LDA, as implemented in CASTEP[36] with the norm-conserving pseudopotential[37], to the band gap calculation in limited cases. The improvement of the band gap result is shown in section IV.

III. BROKEN SYMMETRY STRUCTURES

ScH_3 with the HoD_3 type structure is considered as a starting point. The Sc atoms arrange in the hcp lattice. However, the exact symmetry must be determined from the arrangement of the H_m atoms. There are three possible sites for each H_m atom, i.e. on, under and above the metal plane. As there are six H_m atoms in this unit cell, thus there can be as many as 729 possible arrangements. These arrangements can be view as a wave-like array in [110] direction. By geometrical consideration and also the periodic boundary conditions, they can be reduced to only nine distinguishable arrangements. Then these nine structures are optimized at 0 GPa. We found that only 4 structures, i.e. $P6_3/mmc$, $P\bar{3}c1$, $P6_3cm$ and $P6_3$ as illustrated in Fig. 1, are energetically stable.

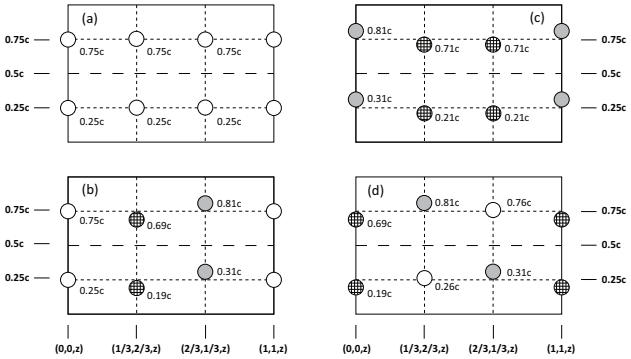

FIG. 1. The H_m atoms are represented by circles of which the symmetry sites are labelled by different marks. They are placed in a unit cell (solid line), and c is along vertical axis. The (x,y,z) are the hexagonal coordinates of atoms on the same vertical line. The figures (a)−(d) are $P6_3/mmc$, $P\bar{3}c1$, $P6_3cm$ and $P6_3$ phases, respectively.

The circles in Fig. 1 represent the positions of the H_m atoms on the (110) plane of the

unit cell. The empty circles are the on-site symmetry positions, and the filled circles are the off-site symmetry positions. The exact coordinates in reduced units are also indicated. In Fig. 1, (a) is the $P6_3/mmc$ phase of which all the H_m atoms are at the on-site symmetry positions, and (b)-(d) are the wave-like arrangement of H_m and can be identified as $P\bar{3}c1$, $P6_3cm$ and $P6_3$ phases, respectively. Among these four structures, the $P6_3/mmc$ structure is the highest symmetry structure with 24 symmetry operations, whereas $P\bar{3}c1$, $P6_3cm$ and $P6_3$ have lower symmetry, i.e. 12, 12, and 6 symmetry operations, respectively. The $P\bar{3}c1$ structure breaks mirror symmetry of $P6_3/mmc$, the $P6_3cm$ structure breaks inversion symmetry, whereas $P6_3$ breaks mirror, inversion and glide symmetries. We shall call these lower symmetry structures as broken symmetry structures from now on. Their optimized lattice parameters are shown in Table. I. Despite of its highest symmetry, the $P6_3/mmc$ energy is more than 0.14 eV higher than those of the broken symmetry structures. For the broken symmetry structures, the energy of $P6_3cm$ is 0.95 meV lower than that of $P\bar{3}c1$. This difference is within our window of the convergence error of 1.6 meV. Thus, $P6_3cm$ and $P\bar{3}c1$ are considered to be equal in terms of energy, i.e. they have a chance to co-exist, similar to the YH_3 case. For simplicity, we choose $P\bar{3}c1$ for discussing the structural comparison. The lowest energy structure is the $P6_3$ phase, where the energy is 8.13 meV lower than the $P\bar{3}c1$ phase. At this stage, the $P6_3$ phase is the strongest candidate for the hcp phase of ScH_3. This conclusion has recently been proposed also by Ye et al.[12] using a structure searching method.

Next, the atomic distribution is considered in order to examine the nature of bondings. To set up a reference, we draw a graphical representation of an Sc atom surrounding by eleven nearest H atoms, composed of three H_m atoms and eight H_t atoms, as shown in Fig. 2(a). According to Table II, upon the symmetry breaking process, the Sc and H atoms are significantly redistributed. The graphical representation in FIG. 2(a) help us keep track of the equivalent H sites in the different structures. The nearest Sc-H_m distance is 1.939 Å in $P6_3/mmc$, and split into 1.954 and 1.958 Å in $P\bar{3}c1$ and split into 1.953, 1.965 and 1.972 Å in $P6_3$, compared with the experimental data of 1.961 Å[23]. The tendency is that the Sc-H_m distances are extended a little along the symmetry breaking process. Furthermore, the electronic population analysis also shows increasing overlap population of Sc-H_m from 0.17 in $P6_3/mmc$, to 0.18 - 0.19 in $P\bar{3}c1$, and to 0.18 - 0.20 in $P6_3$.

TABLE I. The atomic position of the $P\bar{3}c1$, $P6_3cm$ and $P6_3$ phases.

		$P\bar{3}c1$	$P6_3cm$	$P6_3$
Sc		$6f$	$6c$	$6c$
	x	0.664	0.670	0.672
	y			0.006
	z		0.250	0.250
H_t		$12g$	$6c$	$6c$
	x	0.351	0.303	0.374
	y	0.028		0.030
	z	0.091	0.091	0.089
H_t			$6c$	$6c$
	x		-0.355	0.308
	y			0.007
	z		-0.091	0.410
H_m		$2a$	$2a$	$2a$
	z		0.312	0.188
H_m		$4d$	$4b$	$2b$
	z	0.193	0.210	0.263, -0.188

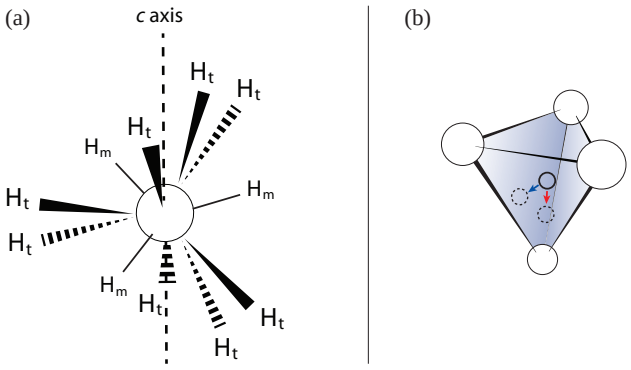

FIG. 2. (a) Bonding between Sc (large circle) with eight H_t and three H_m neighbour atoms. (b) four Sc atoms form a tetrahedron around a H_t atom at the on-site (small solid circle) and the off-site positions (small dash circle). A red (blue) arrow points a direction of the off-site position in the vertical direction (an arbitrary direction). The distances are not to scale.

TABLE II. The distance, d, and the overlap population of orbitals between Sc and H atoms.

	$P6_3/mmc$		$P\bar{3}c1$		$P6_3cm$		$P6_3$	
	d (Å)	overlap population	d (Å)	overlap population	d (Å)	overlap population	d (Å)	overlap population
Sc - H_m	1.939	0.17	1.954	0.18	1.953	0.20	1.953	0.18
			1.958	0.19	1.961	0.19	1.965	0.20
							1.972	0.20
Sc - H_t	2.088	0.12	2.089	0.13	2.088	0.13	2.082	0.13
					2.090	0.13	2.086	0.13
	2.165	0.18	2.293	0.13	2.216	0.16	2.047	0.24
							2.101	0.21
			2.074	0.22	2.084	0.22	2.145	0.18
							2.379	0.11
			2.137	0.20	2.070	0.22	2.331	0.11
					2.341	0.10	2.055	0.23
H_t - H_t	1.927	-0.05	1.963	-0.05	1.967	-0.05	1.988	-0.05
H_t - H_m	2.165	-0.03	2.143	-0.04	2.xxx	-0.04	2.088	-0.04
Sc - Sc	3.358	0.09	3.334	0.11	3.318	0.11	3.320	0.11
							3.338	0.11
							3.413	0.11

In accordance with the H_m arrangements, the H_t atoms are found to displace from the ideal tetrahedral sites to the off-site symmetry positions as well. The H_t atoms in $P6_3/mmc$ phase move to the off-site symmetry positions along the c-axis, as shown by the red arrow direction in FIG. 2(b), whereas in other phases they move to the off-site symmetry positions in a specific direction depended on the phase, as shown arbitrarily by the blue arrow direction in FIG. 2(b). The detail of the H_t displacements varies from phase to phase. However, we focus only on the Sc-H_t distances. The nearest Sc-H_t distance is 2.088 Å in $P6_3/mmc$, and becomes 2.089 Å in $P\bar{3}c1$ and split into 2.082 and 2.086 Å in $P6_3$. This Sc-H_t distance remains almost intact upon symmetry breaking. However, the most intriguing feature is the second nearest Sc-H_t distance of the $P6_3/mmc$ structure. In $P6_3/mmc$, it is 2.165 Å, then split into 2.074, 2.137 and 2.293 Å in $P\bar{3}c1$, and split into 2.047, 2.055, 2.101, 2.145, 2.331 and 2.379 Å in $P6_3$. It is readily seen that the second shell of Sc-H_t in $P6_3/mmc$ is greatly redistributed along the symmetry breaking process. The distribution of the H_t atoms around the Sc atoms causes the variations of the overlap population of Sc-H_t as well. The electronic population analysis shows that the overlap population of Sc-H_t increases from 0.18 at the bond distance of 2.165 Å in $P6_3/mmc$ to 0.24 at the bond distance of 2.047 Å in $P6_3$. This quantity greatly affects the band structure as shall be discussed in section IV.

The experiment reported the Sc-H_t distances at 2.069 and 2.185 Å.[23]

In addition, the distribution among H atoms is also very interesting. The H_t-H_t distance is as close as 1.927 Å in $P6_3/mmc$. Upon symmetry breaking, it is extended significantly to 1.963 Å in $P\bar{3}c1$ and to 1.988 Å in $P6_3$. The experiment reported the H_t-H_t distances at 1.983 Å.[23] Another special feature is the H_t-H_m distance which is 2.165 Å in $P6_3/mmc$. Upon symmetry breaking, the distance of some H_t-H_m pairs is shrinking a little to 2.143 Å in $P\bar{3}c1$, but shrinking significantly to 2.088 Å in $P6_3$. The experiment reported that the nearest H_t-H_m distance is 2.09 Å.[23] We found that the H-H distribution plays an important role in the dynamical stability as shall be discussed in section V.

Segal et al[38] discussed that smaller overlap population tends to be more of the ionic bonding. In ionic crystals, such as NaF and NaCl, the overlap population is about 0.18-0.20, the same order as in Sc-H, but the bulk modulus of ScH_3 is double[6]. In addition, Mullikan charge analysis shows that the Sc charge is around +0.95 whereas the H charge varies between -0.31 and -0.35. This indicates certain degree of ionic bondings in ScH_3 as well. Upon symmetry breaking, the charge of the off-site symmetry H_m atom appears to be a little less negative, while the charge of its three surrounding Sc atoms appear to be a little less positive. For the off-site symmetry H_t atom, the charge remains intact, but the overlap populations among the four surrounding Sc atoms are redistributed. The charge distribution will slightly affect the Madelung energy.

IV. ELECTRONIC PROPERTIES

To analyze the effects of the H arrangements on the electronic properties, the band structures of $P6_3/mmc$ and $P\bar{3}c1$ are compared in Fig. 3(a), and of $P\bar{3}c1$ and $P6_3$ phases are compared in Fig. 3(b). In particular, we consider the band structure in a range of a few eV around the Fermi energy (E_F) only. In this range, the band structure of $P6_3cm$ is quite similar to that of $P\bar{3}c1$. The partial DOS is also evaluated, as shown in Fig. 4. The partial DOS and the characteristic of the band structure help us identify the nature of bands and bondings.

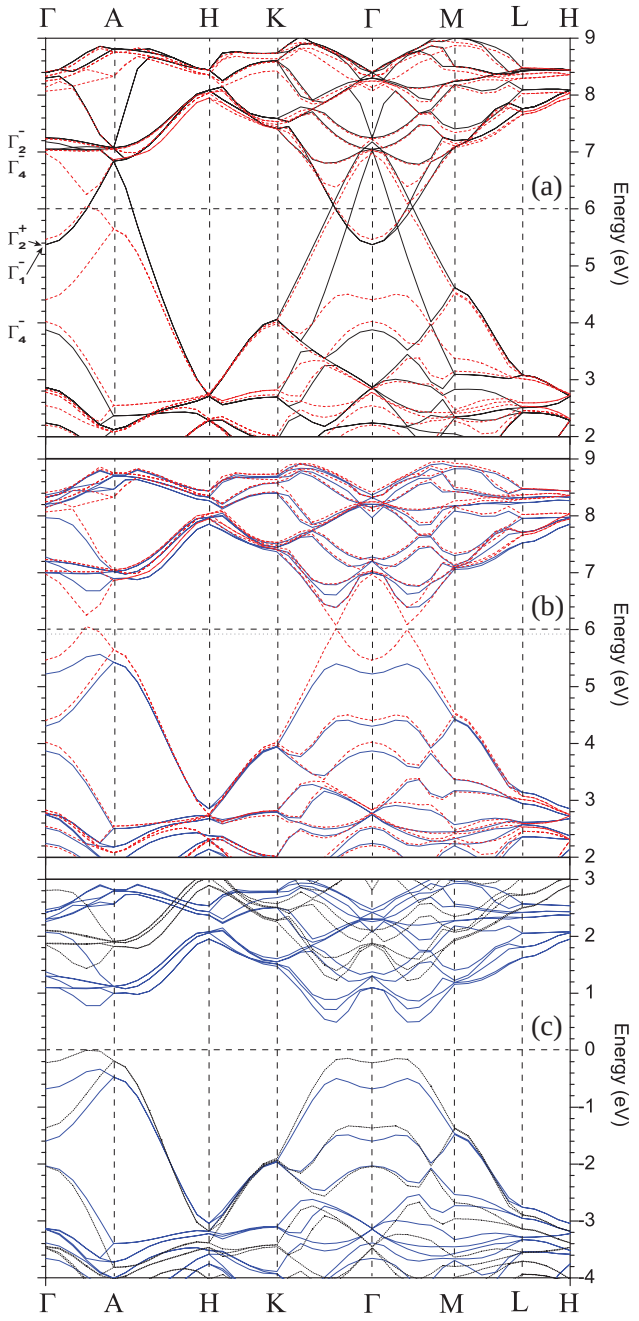

FIG. 3. Comparison of the band structures between (a) $P6_3/mmc$ (black lines) and $P\bar{3}c1$ (red dashed lines) phases and (b) $P\bar{3}c1$ and $P6_3$ (blue line) phases, and (c) $P6_3$ with GGA (blue lines) and with sX-LDA (dotted lines) functionals. The E_F is specified by horizontal dashed lines, but for (c) the E_F is set at 0 eV.

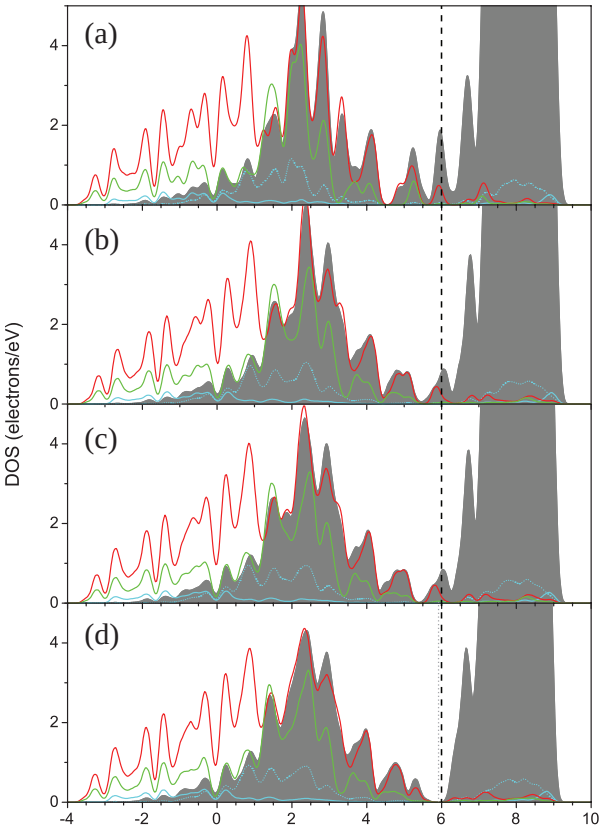

FIG. 4. Partial DOS of (a) $P6_3/mmc$ phase, (b) $P\bar{3}c1$ phase, (c) $P6_3cm$ phase and (d) $P6_3$ phase. The contribution from Sc, H_t and H_m atoms are presented by blue line, red line and green line, respectively. The grey area is from the d orbital of the Sc atom. The solid line and dotted line are the s orbital and the p orbital, respectively.

Let us start with the $P6_3/mmc$ structure which is the highest symmetry among the others. In order to make a compatible comparison, the $P6_3/mmc$ phase is calculated by using the HoD_3-type structure, and placing all the H_m atoms on metal plane, i.e. at the on-site symmetry position. Thus, the Brillouin zone has the same size as the other broken symmetry structures. The partial DOS (FIG. 4(a)) shows that the valance band is dominated by the interactions between Sc and H. By adopting the notations of Wang and Chou[14], they indicated that Γ_1^- (Sc-d_{yz}), Γ_2^+ (Sc-d_{xz}), Γ_2^- (H_t-s), and Γ_4^- (H_m-s and H_t-s) bands are close to E_F, as shown in FIG. 3(a).

Around E_F, the dispersions of Γ_1^- and Γ_2^+ are degenerate. Along Γ-A and K-Γ-M directions, some parts of these two bands are below E_F, and forming electron pockets around the Γ point. At the A point, they raise up to around 0.8 eV above E_F and cross with the

Γ_2^- and Γ_4^- bands. Most of the Γ_2^- and Γ_4^- bands are below E_F, except around the Γ and A points in which the bands raise above E_F, and form hole pockets. The electron and hole pocket manifest themselves as a density peak in the DOS at E_F, as seen in Fig. 4(a). The Γ_1^- and Γ_2^+ bands also cross with the Γ_2^- and Γ_4^- bands at some points along the K-Γ and Γ-M directions. From the band structure, it seems that these four bands are only weakly interacting in $P6_3/mmc$, and it is obvious that there is no band gap in this structure. Thus, the $P6_3/mmc$ structure is a metal. This is in contrast with the optical band gap from the experiment[24] which indicates that ScH_3 is a semiconductor with an extrapolating band gap of 1.7 eV at ambient pressure.

For the $P\bar{3}c1$ and $P6_3cm$ phases, their band structures close to E_F are very similar. However, we shall see later in section V that their phonons are quite different. The band structure is also similar to that of the $P\bar{3}c1$ phase of YH_3 from a previous LDA study[16]. As discussion in the previous section, the wave-like arrangement allows the H_m atoms to occupy the off-site symmetry positions and causes the corresponding rearrangement of the H_t atoms. The H_t atoms in the $P\bar{3}c1$ and $P6_3cm$ phases occupy the off-site symmetry positions as well. The $P\bar{3}c1$ structure breaks mirror symmetry of $P6_3/mmc$, whereas the $P6_3cm$ structure breaks inversion symmetry. Some of the Sc-H_t and Sc-H_m overlap populations are promoted, as seen in Table I, so that their bondings in these broken symmetry structures are stronger than in $P6_3/mmc$. These are consistent with the strong interaction between Γ_1^- and Γ_4^-, i.e. the strong interaction among Sc-d_{yz}, H_m-s and H_t-s. These states are mixed together and open a large gap of about 2.7 eV at the Γ point (see Fig. 3(a)). The partial DOS show that the density peak of Sc, H_t and H_m just below E_F in $P6_3/mmc$ (see FIG. 4(a)) moves to lower energy in $P\bar{3}c1$ and $P6_3cm$, as seen in FIG. 4(b)-(c), respectively. The total energy of $P\bar{3}c1$ and $P6_3cm$ are lowering. The electron and hole pockets are partly removed, i.e. the magnitude of the density peak at E_F is smaller than that of $P6_3/mmc$. Another contribution of the electron and hole pocket comes from the Γ_2^- and Γ_2^+ bands which are only weakly interacting in $P\bar{3}c1$ and $P6_3cm$, and open a much smaller gap of about 0.013 eV. This gap also defines the band gap of these phases. The dispersions of the Γ_2^- and Γ_2^+ interacting bands form cone-like states, as seen in graphene, at approximately half way between K and Γ, and between Γ and M. However, these are removed in the sX-LDA calculation where the d band positions are even higher. We found that the sX-LDA band gaps are 0.158 eV and 0.234 eV in $P\bar{3}c1$ and $P6_3cm$, respectively.

For $P6_3$, the general features of the band structure aound E_F are similar to those of $P\bar{3}c1$ and $P6_3cm$, see the comparison in Fig. 3(b). However, as seen in Table I, some Sc-H_t pairs are getting closer in $P6_3$ than in $P\bar{3}c1$ and $P6_3cm$. The arrangement of H_m in $P6_3$ is now breaking the glide symmetry of $P\bar{3}c1$ and $P6_3cm$. Furthermore, the overlap population of some of Sc-H_t pairs are significantly increased relative to those of the higher symmetry structures. This is because the glide symmetry breaking promotes the strong interaction between the Γ_2^- and Γ_2^+ bands. In the other words, Sc-d_{xz} and H_t-s are now strongly interacting. Consequently, the Γ_2^- and Γ_2^+ interacting bands open an energy gap of about 1.7 eV at the Γ point. From Fig. 4(d), it can be readily seen that the hole pocket is now completely removed, and the electron pocket due to Sc and H_t interaction moves into lower energy, compared with other phases in FIG. 4(a)-(c). Therefore, the E_F and the valence band maximum of $P6_3$ are about 50 meV and 0.5 eV, respectively, lower than those of $P\bar{3}c1$ and $P6_3cm$. This makes the $P6_3$ structure the lowest energy structure among the others. The band gap is now widened to 0.823 eV. The sX-LDA calculation gives the band gap of 1.223 eV. The most improvement from sX-LDA is the position of the d bands of Sc, as seen in FIG. 3(c) Kume et al[24] measured the optical gap of ScH_3 under high pressure, and gave an exterpolation value of the band gap to be 1.7 eV at 0 GPa. A recent work on HSE06 calculation also gave the band gap of 1.55 eV[12]. The electronic stability due to the structural changes and their associated symmetry breaking can be viewed as Peierls distortion in three dimensions.

V. DYNAMICAL PROPERTIES

As we have seen from section III and IV, the $P6_3$ structure is the most energetically favorable, compared with the other three local minimum structures. We need to examine further into their dynamical properties. By using the finite displacement method with a supercell of 192 atoms (48 Sc atoms), we calculate the phonon dispersion (FIG. 5), and the phonon density of states of the $P6_3/mmc$ (FIG. 6), $P\bar{3}c1$(FIG. 7(d)), $P6_3cm$ (FIG. 7(c)) and $P6_3$ (FIG. 7(a)) structures. The phonon density of states is compared with the inelastic neutron scattering (INS) experiment of $ScH_{2.9}$ at 10 K (FIG. 7(c)) by Antonov et al[23].

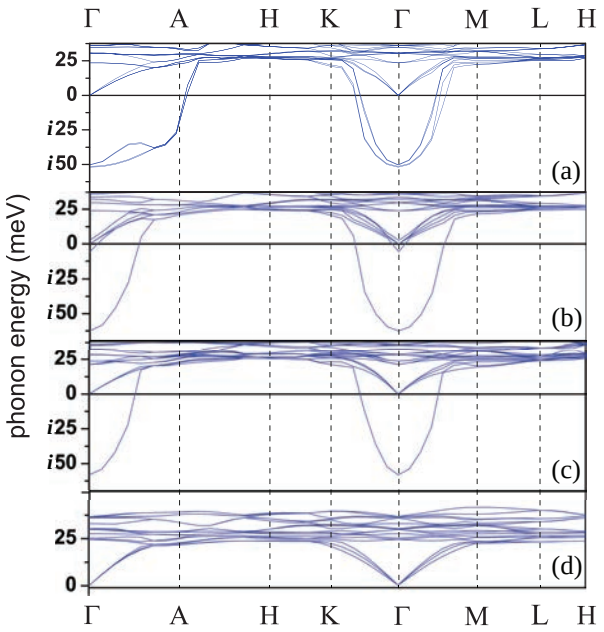

FIG. 5. The phonon dispersion of acoustic modes and optical modes of Sc atoms are presented as follows (a) $P6_3/mmc$, (b) $P\bar{3}c1$, (c) $P6_3cm$ and (d) $P6_3$.

From the calculated phonon dispersion in FIG. 5, the dispersion of the $P6_3/mmc$, $P\bar{3}c1$, and $P6_3cm$ structures exhibit some imaginary modes around the Γ point. Thus, we conclude that only the $P6_3$ structure is dynamically stable. The other structures are unstable. This is in contrast with YH_3 where the $P6_3cm$ structure is also dynamically stable[20]. Our finding could rule out the co-exist phases and the average structure over the co-existing structures, unless the imaginary modes might be stabilized by anharmonic effects at finite temperature.

We examine the phonon density of states in more detail by evaluating the partial phonon DOS, labelled by blue (Sc), green (H_m) and red (H_t) lines in FIG. 6 and FIG. 7. It helps us identify which type of atoms play a major role in a given mode. The phonon DOS of the $P6_3/mmc$, $P\bar{3}c1$, $P6_3cm$ and $P6_3$ structures share some common features. They can be divided into six frequency regions;

1) The Sc region where the vibrations of the Sc atoms dominate. The phonon frequencies of this region are between 0 - 42 meV in all phases. The partial DOS shows some coupling between Sc and H but the vibrations of H are very small in this region. The experimental data[23] shows the peaks between 0 - 45 meV as well, as shown in FIG 7 (b). Due to different responses to neutrons between Sc and H, this part of DOS can be easily assigned to the vibration of the Sc atoms.

2) The *ab*-H_t region where the vibrations with the *ab*-polarization of the H_t atoms dominate. From geometry, the H_t atom is surrounding by four nearest Sc atoms which form a tetrahedron cage. The on-site symmetry H_t atom is located at the center of the tetrahedron. In $P6_3/mmc$, H_t occupies a slightly off-site symmetry position, as shown in FIG. 2(b). The force constants on H_t are moderate, and the frequencies of the *ab*-polarization are between 75 - 125 meV in $P6_3/mmc$. The phonon DOS has very high density around 115 meV. In the broken symmetry structure, H_t occupies another off-site symmetry position, which displaces further from the center of the tetrahedron. This displacement is depending on the structure. The corresponding vibration modes become more complex. Some of the H_t modes are coupled to the H_m modes, and the frequencies shift to lower frequencies in $P\bar{3}c1$, $P6_3cm$ and $P6_3$. Some modes become complicated vibrations with *abc*-polarizations, and the frequencies shift to higher frequencies. The ab-H_t region is confined in the range between 40 - 110 meV. It seems that the high density peak around 115 meV in $P6_3/mmc$ dissociates itself into these two groups, i.e. the H_t-H_m coupling (lower frequencies) and the *abc*-polarization (higher frequencies) regions, in the broken symmetry structures.

3) The *c*-H_t region where the vibrations with the *c*-polarization of the H_t atoms dominate. The *c*-polarization of the H_t modes in the tetrahedron cage show strong interaction, and the frequencies are between 125 - 165 meV in $P6_3/mmc$. Under symmetry breaking process, the H_t atoms experience even stronger interaction, and the frequencies shift to the range between 140 - 170 meV in the broken symmetry structures.

4) The *ab*-H_m region where the vibrations with the *ab*-polarization of the H_m atoms dominate. From geometry, the H_m atom is surrounding by three nearest Sc atoms which form an equilateral triangle. The on-site symmetry H_m atom is located on the plane at the center of the triangle. The interaction on H_m on the plane is very strong and hence the frequencies of the *ab*-polarization are highest , i.e. between 175 - 190 meV in $P6_3/mmc$. The off-site symmetry is located above/below this plane. The force constants are weakening a little, and hence the frequencies of the *ab*-polarization are a little softening to between 170 - 185 meV in $P\bar{3}c1$, $P6_3cm$ and $P6_3$.

5) The *c*-H_m region where the vibrations with the *c*-polarization of the H_m atoms dominate. From section III, the *c*-axis displacements of the H_m atoms along the [110] direction, and all equivalent Γ-M directions, are corresponding to the structural changes. We found also that some of the *c*-polarization of the H_m modes in $P6_3/mmc$ are unstable in Γ-K and

Γ-M directions, see FIG 5 (a). This is because the interaction between Sc and H_m is very weak along the c-axis. Furthermore, the displacement of H_m along the c-axis would lead to a lower energy structure. Thus some components of the force constants may not be well-defined. The phonon DOS is very low in this region between 50 - 70 meV in $P6_3/mmc$. There are some couplings to H_t as well but the density is very low. The unstable modes can be stabilized by the stronger couplings among Sc, H_m and H_t, as seen in the $P\bar{3}c1$, $P6_3cm$ and $P6_3$ structures. The magnitude of the phonon DOS increases. However, it is only $P6_3$ that is fully stabilized.

6) The H_m-H_t region where the coupling vibrations of the Sc, H_m and H_t atoms dominate. The H_m-H_t region is very narrow in $P6_3/mmc$, i.e. between 50-70 meV. However, during the symmetry breaking process, some of the H_m-H_t pairs are getting closer and exhibit stronger interaction, as discussed in section III. Thus the H_m-H_t region shift to higher frequencies and expand to a wider range between 40 - 110 meV in $P\bar{3}c1$, 50 - 105 meV in $P6_3cm$, and 50 - 110 meV in $P6_3$. In $P6_3$, there are five main peaks at 59, 69, 84, 96, 102 meV, compared with the experimental main peaks at 52, 62, 71, 81, 98 and 107 meV[23]. The coupled vibrations in ScH_3 are very crucial to the stability of the hcp phase, and the interactions are just sufficient enough to stabilize $P6_3$ only. Unlike YH_3, where several phases are dynamically stable, thus the stable phase in YH_3 can come from a mixture of the co-exist phases. This mixture will not happen in ScH_3 as the other hcp phases are dynamically unstable and will be quickly transform into $P6_3$.

As discussed above, the calculated peak positions of $P6_3$ phase are generally in good agreement and most comparable with the experimental data[23]. Nevertheless, there is a possibility that the unusually large vibrations of the H atoms at finite temperature and the contribution of anharmonicity need to be taken into account in order to provide more accurate frequencies. Furthermore, the experiment reported with the stoichiometry ratio of x = 2.9(0) for ScH_x. The H defects would also lead to some changes in the normal modes of the system as well. However, these are beyond the scope of the present work.

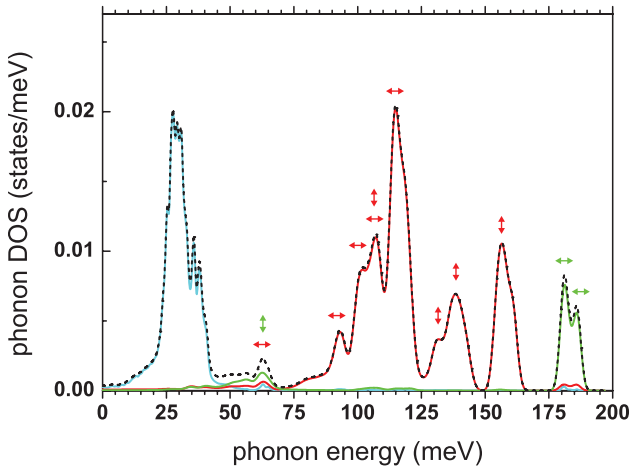

FIG. 6. Partial phonon DOS of the $P6_3/mmc$ phase is presented. The solid lines are the contribution from the Sc atom (blue line), H_t atom (red line) and H_m atom (green line). The total phonon DOS are presented by dashed lines. Vertical arrows denote c-polarization, horizontal arrows denote ab-polarization and crossed lines denote abc-polarization. The polarizations are taken from the modes at Γ point only.

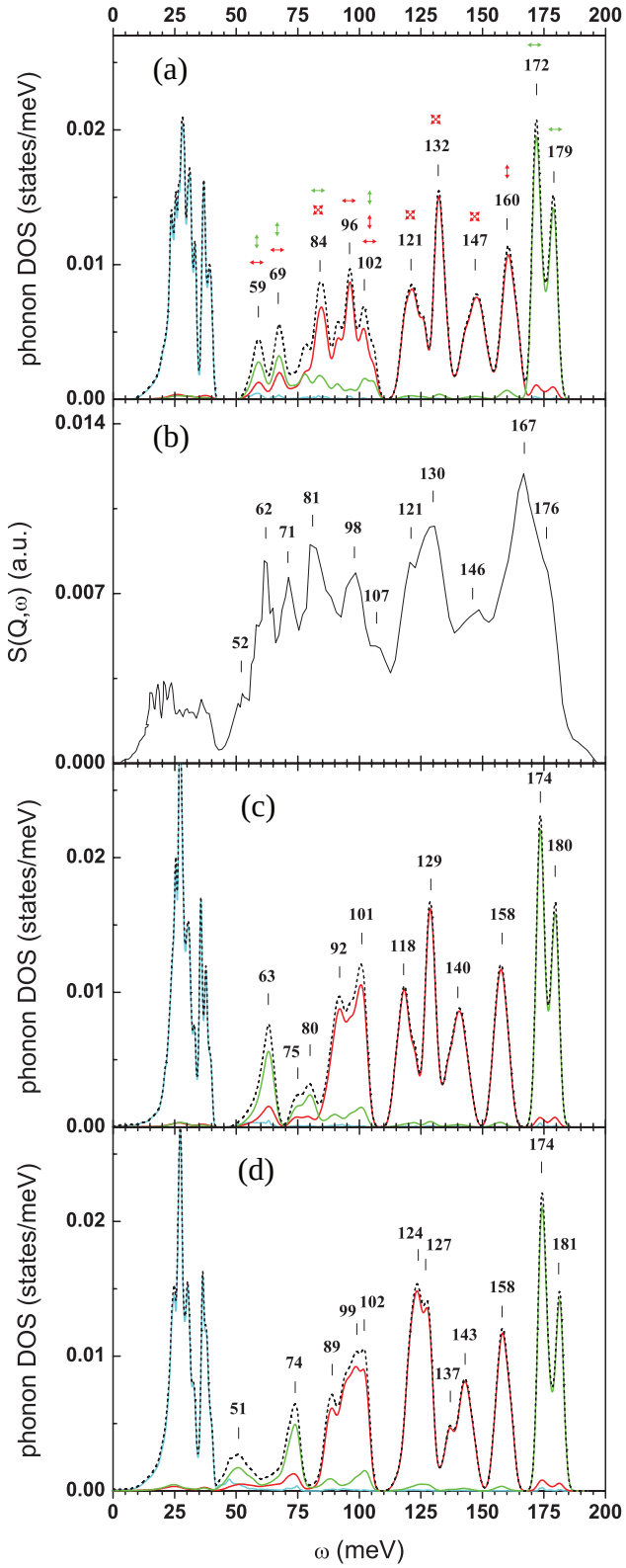

FIG. 7. Partial phonon DOS of (a) $P6_3$ phase, (b) the dynamical structure factor S(Q,ω) from INS experiment, (c) $P6_3cm$ phase and (d) $P\bar{3}c1$ phase. The meanings of lines and the arrows are the same as in Fig. 6.

VI. CONCLUSION

We have used the DFT calculation to study the wave-like arrangements of the H atoms around the metal plane (H_m) in the ScH_3. We found that only the $P6_3/mmc$, $P\bar{3}c1$, $P6_3cm$ and $P6_3$ phases are energetically favorable, but only $P6_3$ is dynamically stable. The wave-like arrangement allows the off-site symmetry positions of the H atoms, and leads to substantial changes in the pair distribution between Sc and H_m, and Sc and H_t, which we have investigated in more detail. There are symmetry breakings along the process. Consequently, the corresponding electronic structure changes in such a way that the total energy is lowering. The symmetry breaking is also responsible for the band gap opening. This mechanism can be viewed as Peierls distortion in 3D. In the $P6_3$ structure, the calculated bandgap is 0.823 eV and 1.223 eV using GGA and sX-LDA functionals, respectively. This band gap can be compared with 1.7 eV derived from the optical measurement and 1.55 eV from the HSE06 calculation[12]. We examined further into the dynamical stability. We found that the stability of $P6_3$ comes from sufficiently strong interactions between two neighboring H_t and H_m atoms. In $P\bar{3}c1$ and $P6_3cm$, these couplings between H_t and H_m are also strong, but not enough to stabilize the phases. This should rule out the co-exist phases or the average structure over the other hcp phases in ScH_3. The calculated phonon density of states of $P6_3$ is in good agreement with the data from the neutron experiment[23]. Some correction could be added due to the large dynamics of H at finite temperature as seen in the Debye-Waller factor in the experiment.

VII. ACKNOWLEDGMENT

We are very grateful to acknowledgement to K. Kotmool for very useful information and discussion. This project has been partially supported by National Research Council of Thailand (NRCT) and National Research University Project, Office of Higher Education Commission (WCU-58-013-FW). T.B. acknowledge TRF contract number RSA5580014. Computing facilities have been partially provided by the Ratchadaphiseksomphot Endowment Fund of Chulalongkorn University (RES260530180-AM) and the Special Task Force for Activating Research (STAR) through the Energy Materials Physics Research Group.

REFERENCES

[1]J. N. Huiberts, R. Griessen, J. H. Rector, R. J. Wijngaarden, J. P. Dekker, D. G. de Groot, and N. J. Koeman, Nature **380**, 231 (1996).

[2]J. N. Huiberts, J. H. Rector, R. J. Wijngaarden, S. Jetten, D. G. de Groot, B. Dam, N. J. Koeman, R. Griessen, B. Hjorvarsson, S. Olafsson, and Y. S. Cho, J. Alloys Compd. **239**, 158 (1996).

[3]R. Griessen, J. N. Huiberts, M. Kremers, A. T. M. van Gogh, N. J. Koeman, J. P. Dekker, and P. H. L. Notten, J. Alloys Compd. **253-254**, 44 (1997).

[4]T. Palasyuk and M. Tkacz, Solid State Commun. **130**, 219 (2004); **133**, 477 (2005); **133**, 481 (2005); **141**, 302 (2007); **141**, 354 (2007).

[5]A. Machida, A. Ohmura, T. Watanuki, T. Ikeda, K. Aoki, S. Nakano, and K. Takemura, Solid State Commun. **138**, 436 (2006).

[6]A. Ohmura, A. Machida, T. Watanuki, K. Aoki, S. Nakano, and K. Takemura, J. Alloys Compd. **446**, 598 (2007).

[7]Y. Yao and D. D. Klug, Phys. Rev. B **81**, 140104 (2010).

[8]Y. Li and Y. Ma, Solid State Commun. **151**, 388 (2011).

[9]B. Kong, L. Zhang, X. R. Chen, T. X. Zeng, and L. C. Cai, Physica B **407**, 2050 (2012).

[10]B. Kong, Z. W. Zhou, D. L. Chen, and R. F. Ling-Hu, Chin. Phys. B **5**, 057102 (2013).

[11]T. Pakornchote, T. Bovornratanaraks, and U. Pinsook, J. Phys. Consds. Matter **26**, 025405 (2014).

[12]X. Ye, R. Hoffmann, and N. W. Ashcroft, J. Phys. Chem. C **119**, 5614 (2015).

[13]T. J. Udovic, Q. Huang, and J. J. Rush, J. Phys. Chem Solids **57**, 423 (1995).

[14]Y. Wang and M. Y. Chou, Phys. Rev. B **51**, 7500 (1995).

[15]R. Eder, H. F. Pen, and G. A. Sawatzky, Phys. Rev. B **56**, 10115 (1997).

[16]P. J. Kelly, J. P. Dekker, and R. Stumpf, Phys. Rev. Lett. **78**, 1315 (1997).

[17]K. K. Ng, F. C. Zhang, V. I. Anisimov, and T. M. Rice, Phys. Rev. B **59**, 5398 (1999).

[18]P. van Gelderen, P. A. Bobbert, P. J. Kelly, and G. Brocks, Phys. Rev. Lett. **85**, 2989 (2000).

[19]P. van Gelderen, P. A. Bobbert, P. J. Kelly, G. Brocks, and R. Tolboom, Phys. Rev. B **66**, 075104 (2002).

[20]P. van Gelderen, P. J. Kelly, and G. Brocks, Phys. Rev. B **63**, 100301 (2001); **68**, 094302 (2003).

[21]V. K. Fedotov, V. E. Antonov, I. O. Bashkin, T. Hansen, and I. Natkaniec, J. Phys.: Condens Matter **18**, 1593 (2006).

[22]T. J. Udovic, Q. Huang, and J. J. Rush, , in Hydrogen in Semiconductors and Metals, edited by N.N. Nickel, W.B. Jackson, R.C. Bowman, and R.G. Leisure, Symposia Proceedings No. 513 (MRS, Pittsburgh, 1998) , 197 (1999).

[23]V. E. Antonov, I. O. Bashkin, V. K. Fedotov, S. S. Khasanov, A. I. Kolesnikov, T. Hansen, A. S. Ivanov, and I. Natkaniec, Phys. Rev. B **73**, 054107 (2006).

[24]T. Kume, H. Ohura, T. Takeichi, A. Ohmura, A. Machida, T. Watanuki, K. Aoki, S. Sasaki, H. Shimizu, and K. Takemura, Phys. Rev. B **84**, 064132 (2011).

[25]S. J. Clark, M. D. Segall, C. J. Pickard, P. J. Hasnip, M. I. J. Probert, K. Refson, and M. C. Payne, Z. Kristall. **220**, 567 (2005).

[26]P. Hohenberg and W. Kohn, Phys. Rev. **136**, B864 (1964).

[27]W. Kohn and L. J. Sham, Phys. Rev. **140**, A1133 (1965).

[28]M. C. Payne, M. P. Teter, D. C. Allan, T. A. Arias, and J. D. Joannopoulos, Rev. Mod. Phys. **64**, 1045 (1992).

[29]J. P. Perdew, K. Burke, and M. Ernzerhof, Phys. Rev. Lett. **77**, 3865 (1996).

[30]D. Vanderbilt, Phys. Rev. B **41**, 7892 (1990).

[31]B. G. Pfrommer, M. Cote, S. G. Louie, and M. L. Cohen, J. Comput. Phys. **131**, 233 (1997).

[32]H. J. Monkhorst and J. D. Pack, Phys. Rev. B **13**, 5188 (1976).

[33]J. D. Pack and H. J. Monkhorst, Phys. Rev. B **16**, 1748 (1977).

[34]W. Frank, C. Elsässer, and M. Fähnle, Phys. Rev. Lett. **74**, 1791 (1995).

[35]A. Seidl, A. Görling, P. Vogl, J. A. Majewski, and M. Levy, Phys. Rev. B **53**, 3764 (1996).

[36]S. J. Clark and J. Robertson, Phys. Rev. B **82**, 085208 (2010).

[37]D. R. Hamann, M. Schlüter, and C. Chiang, Phys. Rev. Lett **43**, 1494 (1979).

[38]M. D. Segall, R. Shah, C. J. Pickard, and M. C. Payne, Phys. Rev. B **54**, 16317 (1996).

Existence of the β-tin structure in Sr: First Evidence from Computational Approach

P. Tsuppayakorn-aek[1,2,3], W. Chaimayo[1], T. Bovornratanaraks[*,1,2,3], U.Pinsook[1,2,3]

[1] Extreme Conditions Physics Research Laboratory (ECPRL), Department of Physics, Faculty of Science, Chulalongkorn University, Bangkok, 10330, Thailand
[2] ThEP, Commission on Higher Education, 328 Si-Ayutthaya Road, 10400, Bangkok, Thailand
[3] Center of Excellence in Forum for Theoretical Science, Department of Physics, Faculty of Science, Chulalongkorn University, Bangkok, 10330, Thailand

Received XXXX, revised XXXX, accepted XXXX
Published online XXXX

Key words: Strontium, Phase transitions, Simulation, Density Functional Theory, Molecular Dynamics.

[*] Corresponding author: e-mail : thiti.b@chula.ac.th, Phone: +66-81-8111750, Fax: +662-253-1150

Molecular Dynamics (MD) calculation is one of the most powerful theoretical methods widely used to predict and to confirm structural phase transitions. In this work, the MD method has been used to verify phase transition from body-centred cubic (bcc) to β-tin structure, then, to the *Cmcm* and hexagonal close-packed (hcp) structure, respectively. The transition sequence from previous theoretical works has been confirmed. In this study, Density Functional Theory (DFT), has been used to calculate phonon dispersion to confirm the stability of β-tin and hcp phases. The long time discrepancies in transition sequence between the calculation and the experimental works has been explained by conventional DFT calculation using screened exchange local density approximation (sX-LDA). More importantly, the existence of β-tin structure is finally predicted and the transition nature of Sr has also been revealed.

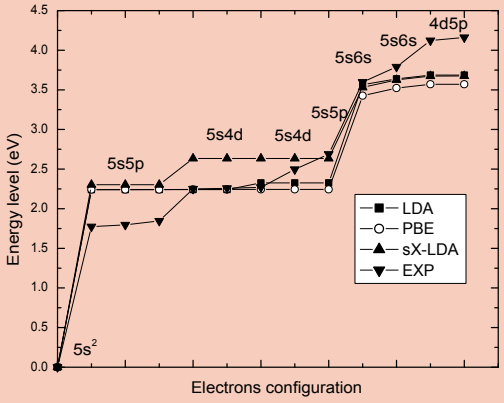

Energy levels in each electron configuration of isolate strontium were calculated using various functional. PBE and LDA functional provide indifferent energy between $5s5p$ and $5s4d$ while the difference is observed in experiment and can be predicted from this calculation using sX-LDA.

1 Introduction Strontium (Sr) is an alkaline-earth metal, which its phase transition under extreme pressure was suggested to be caused by *s*-to-*d* orbital electron transfer from lower pressure to higher pressure phases [1–4]. At ambient pressure, strontium possesses a face-centered cubic (fcc) structure [5] and transforms to a body-centered cubic (bcc) structure at 3.5 GPa [6]. At higher pressure, it transforms to Sr-III at 26 GPa [7], to Sr-IV at 41 GPa [7] and to Sr-V at 46 GPa [7]. The phase Sr-V is stable to at least 74 GPa [10].

Energy-dispersive powder x-ray diffraction experiment carried out by M. Winzenick and W. B. Holzapfel [8] firstly revealed the crystal structure of Sr-III to be orthorhombic structure with spacegroup *Imma* at 31.6 GPa. More importantly, the recent study [9] using full Debye-Scherer angle-dispersive powder x-ray diffraction reinvestigate the crystal structure of Sr-III and identified it to be the tetragonal structure with spacegroup $I4_1$*/amd* named as β-tin structure.

On further compression, McMahon $et\ al.$ [10] were the first who observed Sr-IV phase at above 35 GPa using angle-dispersive powder x-ray diffraction, however, its structure was not yet determined [10]. The Sr-IV structure was later determined to be complex monoclinic structure at 37.8 GPa with space group Ia which can be viewed as the distorted structure of Sr-III, (distorted β-tin structure) by Bovornratanaraks *et al*. [11], using angle dispersive x-ray powder diffraction. In addition, Sr-V was first observed at pressure above 49 GPa and its full structure solution was again determined by McMahon *et al*. [10] to be an incommensurate structure having space group of $I4/mcm$ with atomic positions (x, y = x+1/2, z = 0) where x$\sim$0.15.

Sr has not only been investigated experimentally [9–11], but also computationally [12, 14–16]. In early computational work [12], phase transition in Sr was predicted using the linear-muffin-tin-orbital-atomic sphere approximation method with the combination of nonlocal exchange corrections and the Local-Density Approximation (LDA) which showed that the phase transition of fcc to bcc structure agrees with an experimental work [7]. Recently, the calculation of strontium phases in a medium-pressure-ranged order between 24 GPa and 27 GPa was performed by Srepusharawoot *et al*. [15] using *ab initio* molecular dynamics calculation. In this work, bcc structure is found to transform to *R3c* structure at 27 GPa [15]. However, from the same work [15], by using DFT, enthalpy-pressure relation suggests that the bcc should transform to hcp as the hcp has lower energy compared to that of Sr-IV in 20-30 GPa range [15]. The calculation [15] seemed to disagree with the experiment done by Bovornratanaraks *et al*. [11]. Moreover, the calculations [14, 16] also disagreed with the experiment [11]. In addition, another type of calculation called *ab initio* random structure searching (AIRSS) [17] confirmed that *Cmcm* structure is one of Sr phases existing between 25 GPa - 40 GPa and is confirmed to be stable by Kim *et al*. [16]. In addition, the $Cmcm$ structure will distorts to the hcp structure at 40 GPa [16].

From another $ab\,initio$ calculation by Phusittrakool *et al*. [14], Sr-IV was found to be more stable than the β-tin structure at 20 GPa - 40 GPa range in which the β-tin structure has been experimentally observed [9]. From these evidences, all the theoretical studies of Sr [14–16] show that under high pressure and 0 K, the β-tin structure is a probable structure but not at high temperature (i.e. 300 K). This discrepancy between experimental observation and theoretical prediction have long been unsolved.

In this work, the stability of β-tin and the recently proposed hcp structure [15] will be fully investigated by Density Functional Theory (DFT) and Molecular Dynamics (MD). The discrepancy of the existence of β-tin structure between previous theoretical studies [14–16] and experimental reports [7–11] will be discussed. In addition, the cause of the discrepancy will be illustrated.

2 Method The existence of β-tin structure become doubtful as it was found experimentally [9], however, not theoretically [14–16]. Therefore, there was an attempt [15] to investigate the discrepancy using MD calculations which were purposefully performed at room temperature in order to mimic the conditions used in the experiments [9]. The MD study [15] was established to apply pressure to initial bcc structure which is the lower pressure phase of β-tin structure as reported in [9, 11]. The bcc structure finally relaxed to $R3c$ [15] which is once proposed to be the coexisting phase of β-tin structure [15].

In this work, MD calculations were also established. *NPT*[1] ensembles [19] was employed for the 16-atom system at 300 K and at under the pressure of 30 GPa and 40 GPa when using bcc and β-tin, respectively, as the initial structures. The Brillouin Zone (BZ) were chosen by the Monkhost-Pack mesh (MP) criteria proposed by H. J. Monkhorst and J. D. Pack [20]. In addition, Gamma point (Γ-point) was used as the k-point sampling. The MD calculation showed that the bcc transforms to $Cmcm$ at 30 GPa and the β-tin structure transforms to hcp structure at 40 GPa (see Fig. 1).

To find structural phase transitions, stability of phases and, moreover, to compare with the experimental works [9, 11] and the MD calculations described above, DFT calculations were also performed with some known high-pressure phases of Sr, $i.e.$, fcc [5], bcc [7, 8], β-tin [9], and Sr-IV [11] structures.

DFT calculations were configured to use self-consistent field method, the method to find the ground state energy has been used [23]. Moreover, the Generalized-Gradient Approximation (GGA) of Perdew-Burke-Ernzerhof (PBE) [24] exchange-correlation functional has been employed with ultrasoft psesudopotential [25] which treats $5s^2$, $4p^6$ and $3d^2$ states as valence states. The cutoff energy were set to 700 eV which is optimized to be able to lead the calculation to converge. For the fcc and *Cmcm* structure, the BZ were chosen by the MP mesh resulting in $12\times12\times12$ k-points for fcc, bcc, β-tin, hcp, *Cmcm* structures and $6\times5\times6$ k-point for Sr-IV.

DFT calculations presented in this work were set to perform structural optimization in each pressure increasing step. Enthalpy difference was calculated as the first step for phase transitions identification (see Fig. 2). To find the enthalpy difference between the β-tin and the hcp structures between 20-40 GPa, energy-volume curves

[1] NPT ensemble is the ensemble considering factors, i.e., mole (N), pressure (P),and temperature (T)

were fitted using third order Birch-Murnaghan equation of state [18] . Then the enthalpy was calculated using equation, $H = E+PV$. The intersection point of energy difference curves define phase transition events (see Fig. 2). The existence β-tin and hcp structure were further investigated using phonon dispersion and phonon density of state using energy cutoff of 310 eV, 3×3×5 and 5×5×4 for q-points, and MP 5×5×8 and 9×9×6 for k-point in both β-tin and the hcp structures, respectively. Finite displacement method and super cell scheme using PBE functional at 40 GPa by CASTEP code were employed in these phonon calculations.

From our experience, β-tin and hcp have been the controversial structures among the experiments [9, 11] and the calculation works [15, 16]. They are, therefore, were specially focused. In early calculation work, β-tin and hcp structure used PBE [16] functional. In this work, not only PBE was used in order to reproduce the results [14–16] screened-exchange Local Density Approximation (sX-LDA) [27–29], was also additionally used. Surprisingly, a significant improvement of overall energy was obtained as the overall energy was lowered. Cutoff energy used in this calculation were set to be 660 eV with the norm-conserving pseudo-potential [30] calculation treating $5s^2$, $4p^6$ and $3d^2$ states as the valence states. The brillouin zone (BZ) were chosen by the MP resulting in 3×3×5 and 5×5×4 k-points for both β-tin and hcp structures.

3 Results and Discussion From MD calculation demonstrated using enthalpy-vs-time step plot shown in Fig. 1, bcc structure exhibits the transformation to *Cmcm* structure at 30 GPa and at 300 K. $Cmcm$ structure was also previously determined to have lower enthalpy compared to that of bcc previously calculated using VASP [16]. From these theoretical evidence, $Cmcm$ was shown to exist instead of β-tin structure which was reported to be present in the experimental work done by Allan $et\,al$ [9]. In more profound details, the $Cmcm$ structure has been later explained by burgers mechanism [13] to exist as an intermediate phase of bcc-to-hcp transformation.

The contradiction between experimental discovery [9] and theoretical prediction [15, 16]. β-tin was set as an initial structure and then calculated at 40 GPa and 300 K to find the relaxed structure using MD method with *NPT* ensemble, similarly to what has been done in Fig. 1. The calculation shows that β-tin structure transforms to hcp structure and its stability undergoes from ∼1.5 ps to 5 ps. The calculation consequently suggested that the β-tin structure is not a positive candidate structure.

For DFT calculation, the enthalpy-vs-pressure curves of fcc, bcc, β-tin, Sr-IV, *Cmcm* and hcp structures were shown in Fig. 2. Crossing points of curves from each structure represent the fcc-to-bcc transformation at 1.4 GPa and to hcp structure at 23.8 GPa. In addition, hcp structure (with space group *P6$_3$/mmc*) was found to have lower enthalpy compared to Sr-IV. The hcp structure was found in this calculation but, surprisingly, not in the experiment [9]. The calculation using GGA presented in this work can be validated as it agrees with the previous computational works [15, 16].

From Fig. 2, *Cmcm* and hcp have proximity of enthalpy. However, hcp structure was found to be more energetically favourable than the *Cmcm* structure calculated using MD method. Although the computational resulst described above supports the existence of hcp structure, the hcp structure has not been found experimentally [9]. The disagreement was, therefore, further investigated using phonon dispersions which can verify the stability of hcp and, of course, β-tin structures at 40 GPa.

From Fig. 3, phonon dispersion of the β-tin structure is shown to have the negativity of phonon branch, which is evidenced along Z-to-A, M-to-G (G is Γ-point), G-to-Z, Z-to-R, R-to-X and X-to-G directions. As a result, not only β-tin structure was not shown to be a good candidate for stable structure at 40 GPa, the hcp structure was calculated to have positive phonon frequency which leads the structure to be more favorable (see Fig. 3).

As Sr is an alkaline earth metal, it has been known to have s-to-d orbital electron transfer [1–4] for its phase transition under high pressure. One great example is the transition between bcc to Sr-III [8] was found to have the d-orbital filled when its volume is decreased [4].

In order to investigate the discrepancy mentioned above, various kinds of functional were tested. The functional LDA [26], PBE [24] and sX-LDA [27–29] were used in the DFT calculation. The valence states electrons of strontium were treated as $5s^2$, $4p^6$ and $3d^2$ states.

Energy levels comparison calculated from each functional and also from an experiment [31] were shown in Fig 4. Energy levels were calculated using spin $5s^2$ valence states. One electron spin in 5s is excited and elevated to 5p and, moreover, by having and increasing of energy, an electron spin was then promoted to 4d [28, 29]. In Fig. 4, the calculation from sX-LDA functional demonstrated to have electron configuration corresponding to experiment [31] regarding to the elevation of energy from $5s5p$ to $5s4d$ where the other functionals have indifferent energy between $5s5p$ to $5s4d$ orbitals. It has been demonstrated that the sX-LDA functional can differentiate the energy from $5s5p$ and $5s4d$ [29]

In brife, sX-LDA functional treats d electron differently compared to other functionals [24, 26], PBE and LDA, see Fig 4. The lack of use sX-LDA functional was later found to account for the absence of high-pressure phase, β-tin which was seen in previous theoretical works [14–16]. The sX-LDA functional is then utilized and compared with PBE (see Fig 5) in hcp structure DFT calculation. By using PBE, hcp is shown to be stable which does not agree with experiments reported in [7–9] and computational works reported in [14]. In the contrary, calculation using sX-LDA agreed with those work [9] as β-tin has lower enthalpy and more stable compared to that of hcp.

As sX-LDA can solved some discrepancies between experimental [9] and theoretical works [14–16]. The sX-LDA was use to revalidated the enthalpy different with bcc, hcp and β-tin as shown in Fig. 6. Consequently, β-tin was finally demonstrated for the first time to be more stable than hcp (see Fig. 6) and agree well with experimental result [9]. All in all, this work concludes that sX-LDA is the functional which solved the long-been-discrepancy of β-tin existence.

Even sX-LDA is elaborated to have competence to solve s-to-d orbital problem. It is, however, catch a little attention as no one has used the functional for structural phase transition prediction but for optical [32], band gap [29], band structure electronic density of state [29]. Therefore, this work trailblazes the use of sX-LDA to find structural transition of solids which was validated by solving long-known computational experimental disagreement. Although sX-LDA is proven to be a qualified candidate for alkaline-earth metal, it should also be worth a try for calculation in other elements of this family.

4 CONCLUSION All calculations presented in this work were established to explain high-pressure phases of strontium. Molecular Dynamics (MD) method demonstrated the bcc-to-$Cmcm$ transition at 300 K and 30 GPa and β-tin-to-hcp transition at 300 and 40 GPa. This work originally shows the path transitions of lower-pressure phases→higher-pressure phases, bcc→$Cmcm$ and β-tin→hcp.

In further investigation, DFT was used. Functional PBE was further used to recalculated and revalidated the results from MD. The DFT results demonstrate that the hcp is more energetically favourable than the *Cmcm* structure is and it has lower enthalpy than both the β-tin structure and Sr-IV. As the β-tin structure should actually be the lowest enegy as found presented in experiments [9, 11], further DFT calculation was established using sX-LDA functional. The results from sX-LDA illustrate the existence of β-tin which, for the first time, agree well with experimental work [9].

Acknowledgements This work has been supported by Asahi Glass Foundation, Thailand Center of Excellence in Physics (ThEP), 90^{th} Year Chulalongkorn Scholarship and Ratchadaphiseksomphot Endowment Fund, Chulalongkorn University. T.B. acknowledge TRF contract number RSA5580014. Computing facilities have been partially provided by National Research Council of Thailand (NRCT), the Ratchadaphiseksomphot Endowment Fund of Chulalongkorn University (RES560530180-AM) and the Special Task Force for Activating Research (STAR), Chulalongkorn University through the Energy Materials Physics Research Group.

References

[1] B. Vasvari, A. O. E. Animalu, and V. Heine, Phys. Rev. 154, 535 (1967)
[2] H. L. Skriver, Phys. Rev. Lett. 49, 1768 (1982)
[3] H. L. Skriver, Phys. Rev. B 31, 1909 (1985).
[4] R. Ahuja, B. Johansson, and O. Eriksson, Phys. Rev. B 58, 8152 (1998).
[5] P. W. Bridgman, Proc. Am. Acad. Arts Sci. 72, 207 (1938).
[6] A. Jayaraman, W. Klement, Jr., and G. C. Kennedy, Phys. Rev. 132, 4 (1963)
[7] H. Olijnyk and W. B. Holzapfel, Phys. Lett. 100A, 191 (1984)
[8] M. Winzenick and W. B. Holzapfel, Phys. Rev. B 53, 2151 (1996)
[9] D.R. Allan, R.J. Nelmes, M.I. McMahon, S.A. Belmonte-and,T. Bovornratanaraks, Rev. High Pressure Sci. Tech, Vol. 7, 236-238 (1998)
[10] M.I. McMahon, T. Bovornratanaraks. D. R. Allan, S. A. Belmonteand, R. J. Nelmes, Phys. Rev. B 61, 3135 (2000)
[11] T. Bovornratanaraks. D. R. Allan, S. A. Belmonteand, M.I. McMahon, and R. J. Nelmes, Phys. Rev. B 73, 144112 (2006)
[12] R. H. Mutlu, Phys. Rev. B 54, 16321 (1996)
[13] W. G. Burgers, Physica (Amsterdam) 1, 561 (1934).
[14] A. Phusittrakool, T. Bovornratanaraks, R. Ahuja, and U. Pinsook, Phys. Rev. B77, 1474118 (2008)
[15] P. Srepusharawoot, W. Luo, T. Bovornratanaraks, R. Ahuja, and U. Pinsook, Solid State Commun. 152, 1172 (2012)
[16] D. Y. Kim, P. Srepusharawoot, C. J. Pickard, R. J. Needs. T. Bovornratanaraks, R. Ahuja and U. Pinsook. Appl. Phys. Lett. 101, 052604 (2012)
[17] C. J Pickard and R J Needs 2011 J. Phys.: Condens. Matter 23 053201
[18] F.Birch Phys. Rev. 71, 809824 (1947)
[19] H. C. Andersen , J. Chem. Phys., 72, 2384-2393 (1980)
[20] H. J. Monkhorst and J. D. Pack, Phys. Rev. B. 8213, 5188 (1976)
[21] M. D. Segell, P. J. D. Lindan, M. J. Probert, C. J. Pickard, P. J. Hasnip, S.J. Clark, M. C. Payne, J. Phys.: Condens. Matter 14, 2717 (2002)
[22] S. J. Clark, M. D. Segell, C. J. Pickard, P. J. Hasnip, M. J. Probert, K. Refson, and M. C. Payne, Z. Kristallogr. 220, 567 (2005)
[23] W. Kohn and L. J. Sham, Phys. Rev. A 140, 1133 (1965)
[24] J. P. Perdew, K. Burke, and M. Ernzerhof, Phys. Rev. Lett. 77, 3865 (1996)
[25] D. Vanderbilt, Phys. Rev. B 41, 7892 (1990).
[26] J. P. Perdew and A. Zunger Phys. Rev. B. 23, 5048-5079 (1981)
[27] A. Seidl, A. Görling, P. Vogl, and J. A. Majewski, and M. Levy Phys. Rev. B. 53, 3764 (1996)
[28] B. Lee, L.Wang, C.D. Spataru, S. G. Louie, Phys. Rev. B. 76, 245114 (2007)
[29] S. J. Clark and J. Robertson, Phys. Rev. B. 82, 085208 (2010)
[30] D. R. Hamann, M. Schlter, and C. Chiang, Phys. Rev. Lett., 43, 1494-1497 (1979).
[31] C. E. Moore, Atomic Energy Levels, Natl. Bur. Stand. (U.S.) Circ. 467, Vol. II (1952); reprinted as Natl. Stand. Ref. Data Ser., Natl. Bur. Stand. (U.S.) 35 (1971).
[32] M. Kim, Y. J. Zhao, and A. J. Freeman and W. Mannstadt, Appl. Phys. Lett. 84, 3579 (2004)

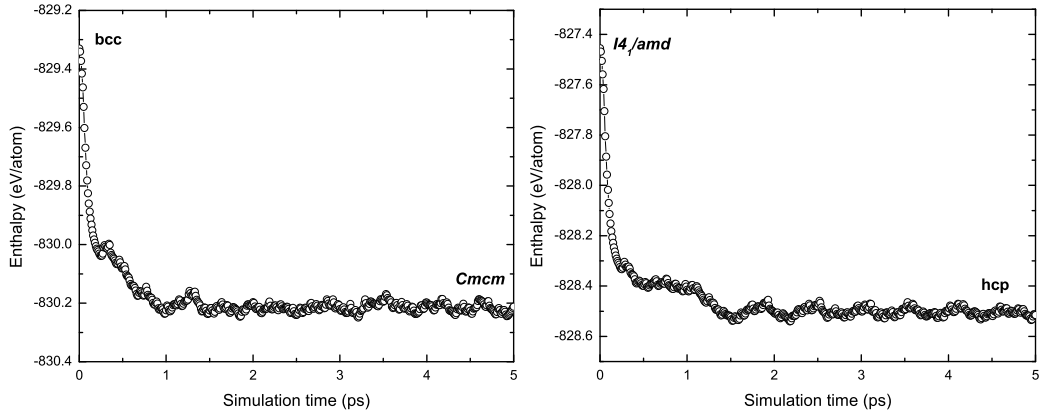

Figure 1 (left) Bcc super cells structure was calculated using MD simulation resulting in the appearance of $Cmcm$ structure at a few picoseconds after the simulation has started. (right) the similar MD calculation was also established with $I4_1$*/amd* super cells as a starting structure. After a few second, the appearance of hcp structure was observed. These graphs suggest that $Cmcm$ is more stable than bcc (left) and hcp is more stable than $I4_1$*/amd* (right) at temperature 300 K.

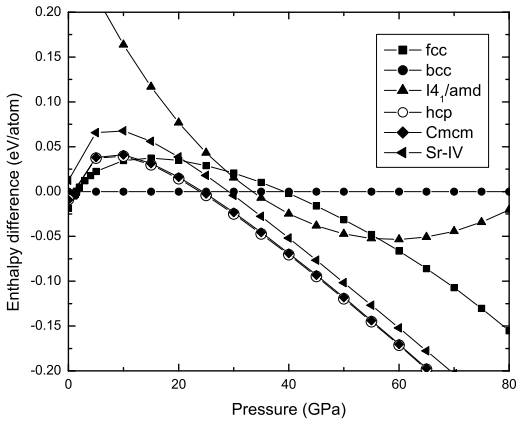

Figure 2 The enthalpy difference of fcc, β-tin, hcp, Sr-IV, and *Cmcm* structure related to the bcc structure at ambient pressure. The crossection point of each line represents the occuring of transition event. The graph suggests that the transition will go from fcc $\rightarrow$ bcc $\rightarrow$ hcp.

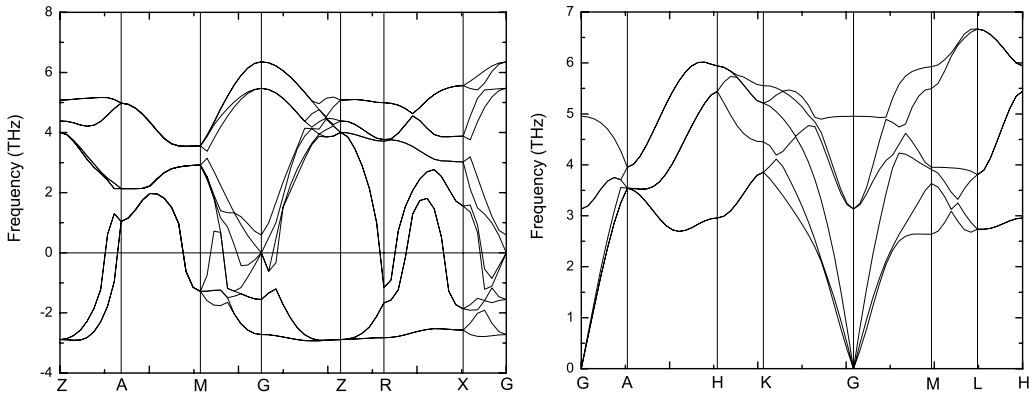

Figure 3 (left) Phonon dispersion and density of phonon state of β-tin at 40 GPa calculated using PBE functional. The negative phonon can be interpret that the structure is unlikely to be stable and (right) those of hcp structure at 40 GPa was also calculated using PBE functional. The positive phonon branch suggests the stability of the structure.

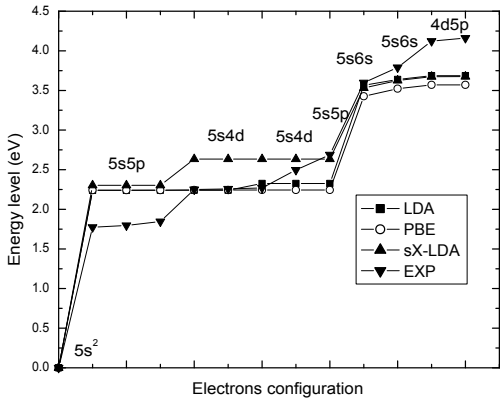

Figure 4 Energy levels in each electron configuration of isolate strontium were calculated from LDA, PBE, and sX-LDA . PBE and LDA functional provide indifferent energy of $5s5p$ and $5s4d$ while the difference is found in experiment [31] and also from the calculation using sX-LDA.

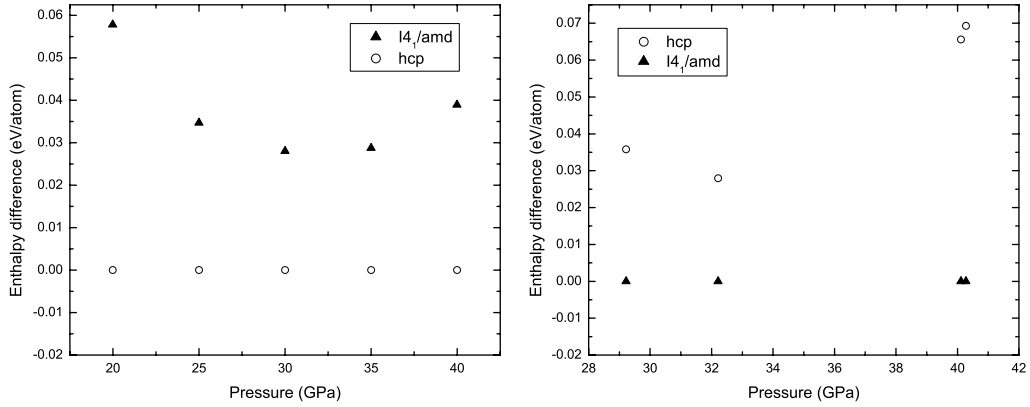

Figure 5 (left) The enthalpy different of β-tin to hcp structure calculated using PBE and (right) the enthalpy different of hcp stucture to β-tin using sX-LDA.

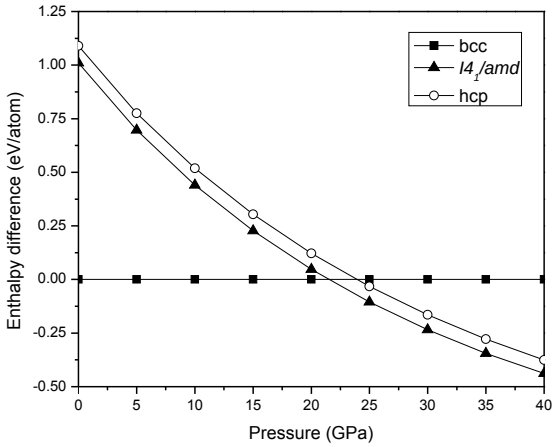

Figure 6 The enthalpy different of $I4/amd$ and hcp from bcc structure calculated using sX-LDA functional are illustrated. The curves suggest the better stability of $I4/amd$ over hcp structure which agrees with the experiment [9]. The graph shows that the transition from the bcc structure to the β-tin structure at pressure 21.4 GPa.